The Role of Galectin-3: From Oligodendroglial Differentiation and Myelination to Demyelination and Remyelination Processes in a Cuprizone-Induced Demyelination Model

H.C. Hoyos, Mariel Marder, R. Ulrich, V. Gudi, M. Stangel, G.A. Rabinovich, L.A. Pasquini and J.M. Pasquini

Abstract The aim of this work was to combine our previously published results with our new data to show how galectin-3 (Gal-3) controls myelin integrity and function, promotes oligodendroglial cell differentiation, and regulates microglial responses to limit cuprizone- (CPZ)-induced demyelination and foster remyelination. In this study, 8-week-old Gal-3-deficient (*Lgals3*$^{-/-}$) and wild type (WT) mice were fed a diet containing 0.2 % CPZ w/w for 6 weeks, after which CPZ was withdrawn in order to allow remyelination. Our results show that remyelination was less efficient in *Lgals3*$^{-/-}$ than in WT mice. Electron microscopic images from remyelinated sections in *Lgals3*$^{-/-}$ mice revealed collapsed axons with a defective myelin wrap, while remyelinated WT mice had normal axons without relevant myelin wrap disruption. MMP-3 expression increased during remyelination in WT but not in *Lgals3*$^{-/-}$ mice. The number of CD45+, TNFα+ and TREM-2b+ cells decreased only in WT mice only, with no alterations in *Lgals3*$^{-/-}$ mice during demyelination and remyelination. Therefore, Gal-3 influences remyelination by

L.A. Pasquini and J.M. Pasquini contributed equally to this work and should be considered as co-senior.

H.C. Hoyos · M. Marder · L.A. Pasquini · J.M. Pasquini
Department of Biological Chemistry, School of Pharmacy and Biochemistry, Institute of Chemistry and Biological Physical Chemistry (IQUIFIB), Buenos Aires, Argentina

H.C. Hoyos · M. Marder · L.A. Pasquini · J.M. Pasquini
School of Pharmacy and Biochemistry, University of Buenos Aires and National Research Council (CONICET), Buenos Aires, Argentina

R. Ulrich
Department of Pathology, University of Veterinary Medicine Hannover, Hannover, Germany

V. Gudi · M. Stangel
Department of Neurology, Hannover Medical School, Hannover, Germany

R. von Bernhardi (ed.), *Glial Cells in Health and Disease of the CNS*,
Advances in Experimental Medicine and Biology 949,
DOI 10.1007/978-3-319-40764-7_15

mechanisms involving the tuning of microglial cells, modulation of MMP activity, and changes in myelin architecture.

Keywords Galectin-3 · Myelination · Demyelination · Remyelination · Cuprizone · Microglia · Oligodendrocytes · MMPs

Abbreviations

MMPs	Matrix metalloproteinases
Gal-3	Galectin-3
Lgals3$^{-/-}$	Gal-3-deficient
WT	Wild type
CPZ	Cuprizone
CRD	Carbohydrate-recognition domain
CNS	Central nervous system
OLG	Oligodendrocyte
EAE	Experimental Autoimmune Encephalomyelitis
CC	Corpus callosum
OPC	Oligodendrocyte precursor cells
MBP	Myelin basic protein
PBS	Phosphate buffered saline
PFA	Paraformaldehyde
SVZ	Subventricular zone
EM	Electron Microscopy
GFAP	Glial Fibrillary Acidic Protein
IOD	Integrated optical density

V. Gudi · M. Stangel
Center for System Neurosciences, Hannover, Germany

G.A. Rabinovich
Laboratory of Immunopathology, Institute of Biology and Experimental Medicine (IBYME; CONICET), C1428 Buenos Aires, Argentina

G.A. Rabinovich
Laboratory of Functional Glycomics, Department of Biological Chemistry, Faculty of Exact and Natural Sciences, University of Buenos Aires, C1428 Buenos Aires, Argentina

L.A. Pasquini · J.M. Pasquini (✉)
Dpto. de Qca Biol, FFyB-UBA, Junín 956, C1113 Bs as, Argentina
e-mail: jpasquin@qb.ffyb.uba.ar

Introduction

Galectins belong to a family of β-galactoside-binding lectins. Although they lack specific receptors, they can form multivalent complexes by binding to cell surface glycoconjugates containing suitable oligosaccharides and generate intracellular signals in order to regulate cell survival and differentiation (Rabinovich et al. 2007; Yang et al. 2008). In the immune system, galectin-1 and -3 (Gal-1and Gal-3, respectively) often have antagonistic roles in the modulation of adaptive immunity, with Gal-3 being predominantly proinflammatory and Gal-1 anti-inflammatory (Rabinovich and Toscano 2009). Gal-3, a chimeric protein with many actions, including modulation of innate and adaptive immunity, has unusual tandem repeats of proline and glycine-rich in short stretches fused to a carbohydrate-recognition domain (CRD) (Rabinovich and Croci 2012).

Although the function of Gal-3 in central nervous system (CNS) immunity has not been elucidated, most in vitro and in vivo studies hint at a proinflammatory role in the promotion of immune cell activation, migration and inhibition of apoptosis (Rabinovich et al. 2007), although negative regulation of lipopolysaccharide-induced inflammation has also been proposed (Li et al. 2008). Our group first studied the relevance of galectin–glycan lattices in oligodendrocyte (OLG) physiology and identified an essential role for galectin–glycan interactions in regulating OLG differentiation, leading to control of myelin integrity and function. We found that astrocytes and microglia have high expression of both Gal-1 and -3. In contrast, while immature OLGs but not differentiated OLGs highly expressed Gal-1, differentiated OLGs expressed Gal-3. Matrix metalloproteinases (MMPs) activity increased, thereby processing Gal-3 during OLG differentiation and regulating its biological activity. Recombinant Gal-3 treatment accelerated OLG differentiation in a dose- and carbohydrate-dependent manner, in accord with the "glycosylation signature" of immature versus differentiated OLGs. Furthermore, conditioned media from Gal-3-expressing, but not Gal-3-deficient ($Lgals3^{-/-}$) microglia, induced OLG differentiation. Supporting these findings, morphometric analyses revealed a significant reduction in the number of myelinated axons and myelin turns (lamellae), as well as in the g-ratio of $Lgals3^{-/-}$ mice. Moreover, myelin sheaths were more loosely wrapped around axons in $Lgals3^{-/-}$ mice. $Lgals3^{-/-}$ mice had lower anxiety levels, like those during early cuprizone (CPZ)-induced demyelination. In addition, neurospheres isolated from WT but not from $Lgals3^{-/-}$mice favored commitment to oligodendroglial fate. Together, these results indicate that glial-derived Gal-3, but not Gal-1, promotes oligodendroglial differentiation and thus contributes to myelin integrity and function, which has critical implications in the recovery of inflammatory demyelinating disorders (Pasquini et al. 2011).

Within the CNS, Gal-3 is upregulated by inflammatory stimuli and is harmful in prion-infected brain tissue (Mok et al. 2006, 2007; Riemer et al. 2004). On the other hand, Gal-3 mediates the activation and proliferation of microglia in a focal cerebral ischemia model in mice (Lalancette-Hébert et al. 2012). In experimental autoimmune encephalomyelitis (EAE), an animal model of CNS demyelination in which

mice are immunized with myelin OLG glycoprotein, Jiang et al. (2009) reported a decreased severity in Lgals3$^{-/-}$ animals. In contrast, administration of CPZ in the diet of young adult mice causes extensive demyelination in several areas of the CNS, particularly in the corpus callosum (CC), independently of pathogenic T cells (Matsushima and Morell 2001). CPZ-induced demyelination increases the number of resident microglia and the presence of few peripheral macrophages (Masuda-Nakagawa et al. 1993; von Bernhardi and Muller 1995; McMahon et al. 2002). These microglia have been reported to phagocytize myelin, associated with the upregulation of phagocytic receptors among which TREM-2b is the most prominent (Voß et al. 2011). Remarkably, considering that myelin can inhibit the differentiation of oligodendrocyte precursor cells (OPC), this phagocytosis has been proposed to play a key role in the onset of remyelination (Kotter et al. 2006).

We have recently published a manuscript comparing CPZ-induced demyelination in 8-week-old *Lgals3*$^{-/-}$ and WT mice. Our findings showed that *Lgals3*$^{-/-}$ and WT mice are similarly susceptible to CPZ until treatment week 5, as evaluated by myelin basic protein (MBP) immunelabeling and electronic microscopy. However, OPCs generated in CPZ-treated *Lgals3*$^{-/-}$ mice showed diminished arborization, which suggests a decrease in differentiation capability. Surprisingly, while WT mice experienced spontaneous remyelination by week 5, even though the CPZ diet was maintained to week 6, *Lgals3*$^{-/-}$ mice lacked this capacity and remained demyelinated to week 6, with pronounced astroglial activation. Behavioral studies of WT and *Lgals3*$^{-/-}$ mice found lower innate anxiety after 2 weeks of CPZ treatment, but only *Lgals3*$^{-/-}$ mice had decreased locomotor activity and impaired spatial working memory. Gal-3 expression increased during CPZ-induced demyelination in microglia but not in astrocytes. Interestingly, microglial activation, ED1 expression, and phagocytic receptor TREM-2b levels increased only in CPZ-treated WT mice. In contrast, CPZ-treated *Lgals3*$^{-/-}$ mice showed an increased number of microglia with caspase-3 activation. Taken together, our results indicate that Gal-3 is expressed in microglial cells to modulate their phenotype during CPZ-induced demyelination (Hoyos et al. 2014).

Multiple sclerosis (MS) is a CNS disease leading to the demyelination of white and gray matter (Stadelmann 2011) (see Chapter "Peripheral Inflammation and Demyelinating Diseases"). Remyelination is the regenerative response to demyelination (Franklin and Kotter 2008); it is characterized by thinner axons and myelin sheaths. Although the complex biological interactions underlying remyelination are still not clear, the process is known to involve the proliferation of OPCs, their subsequent migration toward demyelinated axons and their final differentiation (Franklin and Ffrench-Constant 2008), all steps regulated by intrinsic and extrinsic factors.

MMP are a family of zinc-dependent endopeptidases which, together with endogenous tissue inhibitors of MMP, play essential roles in tissue remodeling. MMPs can degrade myelin proteins in vitro (Chandler et al. 1995, 1996; Shiryaev et al. 2009; Hansmann et al. 2012) and are suggested to be involved in the initiation of demyelination in vivo (Hansmann et al. 2012; Ulrich et al. 2006; Skuljec et al. 2011). Furthermore, both MMP and their inhibitors have been implicated in

postnatal myelination, myelin maintenance, and remyelination (Skuljec et al. 2011; Ulrich et al. 2005).

In this work, to further analyze the role of Gal-3 in the control of the glial cell response to a demyelination insult, we have assessed the involvement of Gal-3 in the control of the remyelination process after CPZ-induced demyelination. To this end, we have analyzed the expression of different markers of the oligodendroglial lineage and performed morphometric analyses of electron micrographs. We have also evaluated the astroglial response, as well as changes in the microglial phenotype and the expression of MMP-3 in the CC during remyelination.

Experimental Procedures

Animals and Experimental Model

Lgals3$^{-/-}$ mice (C57BL/6 background) were generously provided by Dr. Fu-Tong Liu (University of California, Davis, USA) and generated as previously described (Hsu et al. 2000). Animals were housed in groups of 4 in a controlled environment (20–23 °C) with free access to food and water and maintained in a 12 h/12 h day/night cycle, with light on at 6 am. All animal protocols were approved by the Institutional Review Board of the University of Buenos Aires and animal experimentation was in accordance with the National Institutes of Health Guide for the Care and Use of Laboratory Animals.

Experimental demyelination was induced by feeding 8-week-old male mice with 0.2 % (w/w) CPZ (bis-cyclohexanone oxalhydrozone; Sigma Aldrich, Saint Louis, USA) mixed into standard ground rodent chow (Matsushima and Morell 2001). These mice were fed CPZ for 6 weeks and then allowed to remyelinate for 2 additional weeks. Studies, including weight measurements, were done fot 5 weeks (the point of maximum demyelination) and during the remyelination period. The demyelination–remyelination protocol is summarized in Fig. 1a.

Slice Preparation and Brain Section Selection

Animals were anesthetized with a xylazine–ketamine mixture and intracardially perfused with 30 ml phosphate buffered saline (PBS), pH 7.4, followed by 4 % paraformaldehyde (PFA, Sigma Aldrich, Saint Louis, USA) in PBS, pH 7.4. Brains were carefully dissected out, post-fixed in the same solution overnight and later thoroughly washed in PBS and cryoprotected in 30 % sucrose in PBS. All brain slices (25-μm width) were kept at −20 °C in a PBS-glycerol solution (1:1) until used for immunofluorescence studies.

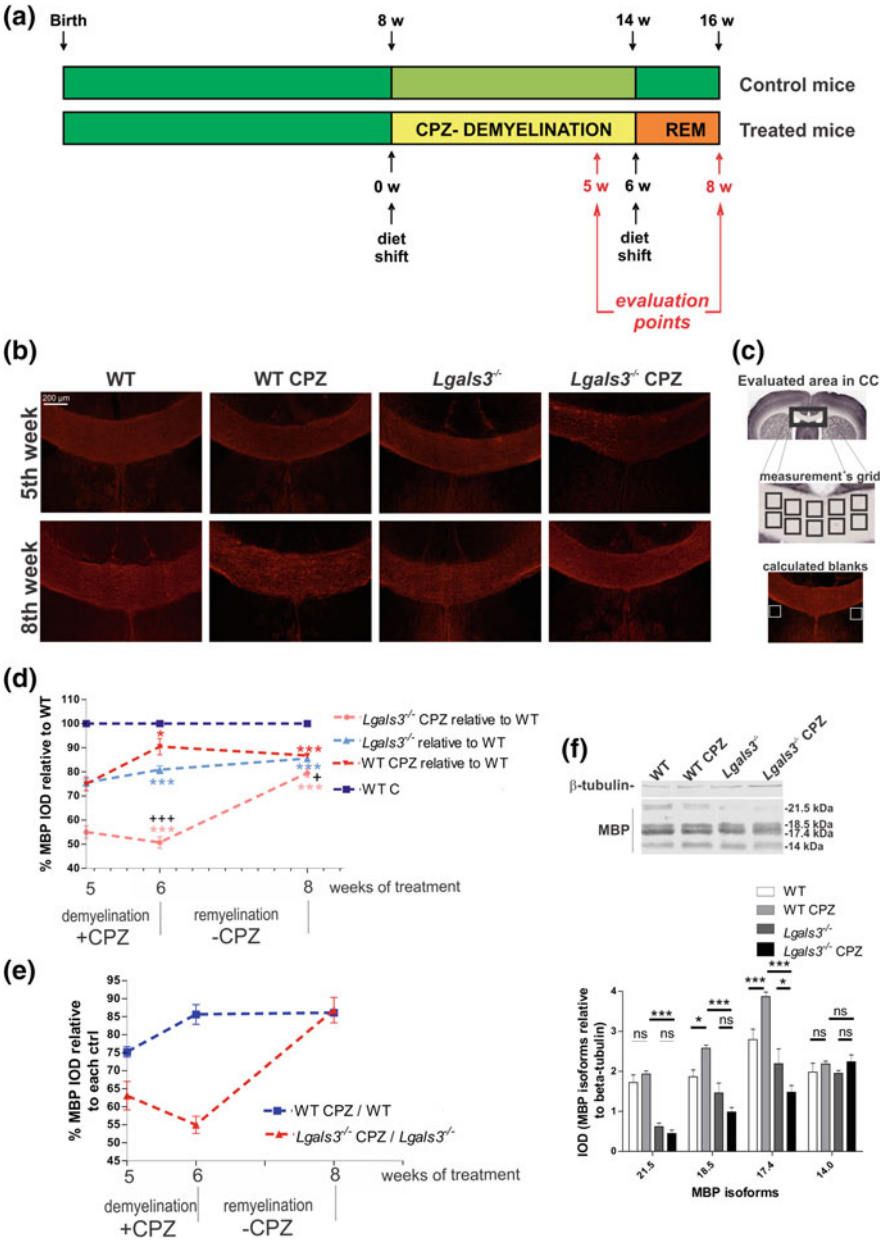

Previous to immunostaining, brain slices were selected using the Allen Mouse Brain Atlas as a reference. The corpus callosum (CC) and subventricular zone (SVZ) were studied in brain sections at the level of coronal slices 44–52 of the Atlas. After selection, brain slices were kept in PBS for immunohistochemical

◀ **Fig. 1** **a** Schematic illustration of the experimental design. Two evaluation points were determined (5th week of demyelination and 8th week—2 weeks after CPZ withdrawal from the diet). **b** Representative sections showing MBP expression in stained CC sections at the 5th week of treatment and 2 weeks after CPZ withdrawal (8th week). **c** Immunoreactive signal measured by IOD in a grid of ten 1-mm^2 rectangles, as detailed in the scheme (*box*) using Image Pro Plus 5.5 software. Blanks for IOD were calculated in the zones indicated by white boxes in the representative image. Images (magnification 10×) were obtained from 5 mice per treatment per time point. **d** Demyelination score at the 5th week measured by MBP IOD (WT is 100 %). **e** Remyelination rate during treatment of WT CPZ relative to WT mice and *Lgals3*$^{-/-}$ CPZ relative to *Lgals3*$^{-/-}$ mice. **f** Western blot analysis of MBP expression during remyelination. Samples were taken from CC at the 8th week. β-tubulin was used as a loading control. Values represent the mean ± SEM of five independent experiments. $*p < 0.05$, $**p < 0.01$, $***p < 0.001$ using one-way analysis of variance (ANOVA) followed by Bonferroni post hoc tests

studies. For electron microscopy (EM) and flow cytometry (isolation of microglia), the CC was dissected out from brains kept on ice using a sterile razor blade. Dissection coordinates were +1.32 mm to +0.74 mm from Bregma, according to The Mouse Brain Library. The isolated CC was immediately subjected to procedures required for each particular assay.

Immunohistochemistry

Cryosections were rinsed twice with PBS (pH 7.4) and then treated with an antigen-blocking reagent composed of 5 % FCS and 0.1 % Triton X-100 in PBS. Primary and secondary antibody dilutions were prepared in 1 % FCS and 0.1 % Triton X-100 in PBS. Primary antibody incubations were done overnight at 4 °C. The primary antibodies used were rabbit anti-MBP (1/600; generously provided by Dr. A. Campagnoni, UCLA, Los Angeles, USA); rabbit anti-CAII (1/400; generously provided by Dr. W. Cammer, A. Einstein College of Medicine, New York, U.S.A.); mouse anti-CC1 (1/100, Abcam, Massachusetts, USA); goat anti-PDGFRα (1/100, Neuromics, Edina, USA); chicken anti-Glial Fibrillary Acidic Protein (GFAP) (1/100, Neuromics, Edina, USA); mouse anti-MMP-3 (1/100, Calbiochem), generously provided by Dr. Alicia Jawerbaum (CEFYBO, UBA, Buenos Aires, Argentina); and goat anti-Iba-1 (1/100, Abcam, Massachusetts, USA). Incubation with Hoechst 33342 (Sigma Aldrich, Saint Louis, USA) and various fluorescent secondary antibodies (Alexa 488, Alexa 649, Cy2 and Cy3, Jackson Immunoresearch Lab, Argentina) was done for 2 h at 37 °C with agitation. Slides were mounted and covered with Mowiol. Microphotographs were taken with an Olympus BX50 epifluorescence microscope connected to a CoolSnap digital camera.

Image Pro Plus software (version 5.5) was used for image analysis. For MBP and MMP-3, integrated optical density (IOD) was measured in CC. Figure 1c illustrates the measurement method. Ten squares (surface equal 1 mm^2) were displayed per image and IOD was calculated and averaged in each square for each

image. For the remaining markers, the number of positive cells was counted in each case using Image J software and validated through manual count by an experimenter who was blind to the experimental design.

For CAII, CC1, PDGFRα, MMP-3, and Iba-1 images, observations were carried out using an Olympus Fluorview FV1000 MPE multiphoton microscope coupled to a Zeiss LSM 510 laser scanner. Merged versions and composite images were obtained with FV10-ASW1.7 viewer software (Olympus). Filament plots of PDGFRα and Iba-1 cells were obtained from z-stack scanning of cells at a slice distance of 0.75 μm using the IMARIS 6.3.1 program (Bitplane Sci Software) as previously described (Hoyos et al. 2014).

Western Blot Analysis

MBP isoforms and GFAP were evaluated in CC cell extracts. Samples were resuspended and lysed in RIPA 1 × (NaCl 300 mM, TRIS 20 mM, pH.7.4, SDS 0.2 %) extraction buffer with a complete EDTA-free protease inhibitor cocktail (Roche). Equal amounts of protein were separated on SDS-PAGE and transferred onto PVDF membranes for Western blot analyses. Membranes were incubated with anti-MBP (1/1000) and anti-GFAP (1/1000) antibodies, followed by incubation with HRP-conjugated antibodies. Quantification was done by densitometry with the Gel Pro Analyzer 4.0 system.

Electron Microscopy

Four to six animals per group were decapitated. CC were dissected out as described above, fixed and immediately prepared for EM. Ultrathin cuts were examined using a Zeiss Leo 906 E electron microscope equipped with a Zeiss Megaview III digital camera. Parameters assessed included: (a) percentage of correctly myelinated axons per field; (b) g-ratio (the ratio between the axon's diameter and the axon's diameter wrapped with myelin); and (c) number of myelin turns around an axon. Images were analyzed by experimenters who were blind to the experimental design. Eight images were obtained for each experimental condition.

Isolation of Microglia

Isolation of microglia was carried out as described by Hoyos et al. (2014).

May Grünwald Giemsa Staining

Coronal brain slices of remyelinated *Lgals3*$^{-/-}$ and WT mice were washed in distilled water to remove PBS/glycerol, preserved and mounted on glass. When slices were completely attached to glasses, they were washed twice again and incubated for 90 s with May Grünwald reagent (Biopack, Buenos Aires, Argentina). Afterwards, slices were washed four times for 2 min each, then incubated 20 min in Giemsa dye (Biopack, Buenos Aires, Argentina) and rewashed four more times for 2 min each. Both reagents were generous gifts of Dr. Miriam Lardone (Hospital de Clínicas "José de San Martín", Buenos Aires, Argentina).

Behavioral Tests

Assessment of behavioral performance following remyelination was carried out as described by Hoyos et al. (2014).

Statistical Analysis

Graph-Pad Prism software was used for data analysis. Results were presented as the mean ± standard error of the mean (SEM). Comparisons were performed using unpaired two-tailed Student's *t*-test or two-way analysis of variance (ANOVA), followed by Bonferroni's post hoc tests when appropriate. Values of $p < 0.05$ (*), $p < 0.01$ (**), $p < 0.001$ (***) were considered significant.

Data from behavioral assays were analyzed by two-way ANOVA, considering CPZ treatment and animal type as two main factors, and post hoc comparisons were made using Bonferroni's post-test. When a significant interaction was observed, subsequent one-way ANOVA and Newman-Keuls Multiple Comparison post hoc test were applied. A value of $p < 0.05$ was considered statistically significant.

Results

Remyelination Starts Earlier in WT CPZ Than in Lgals3$^{-/-}$ *CPZ Mice but Reaches the Same Endpoint*

To study the impact of Gal-3 deficiency on the remyelination process, WT and *Lgals3*$^{-/-}$ mice were submitted to demyelination through a diet containing 0.2 % (p/p) CPZ for 6 weeks and then studied after 2 weeks on a normal diet (Fig. 1a).

Animals were sacrificed at the critical point of demyelination (5th week) and after 2 weeks' remyelination (8th week).

MBP immunelabeling was carried out in WT and *Lgals3*$^{-/-}$ mice at the critical point of demyelination and at the end of remyelination (Fig. 1b). MBP IOD measurements during remyelination relative to WT showed that WT CPZ mice experienced spontaneous remyelination from the 5th week of treatment (when CPZ was still in the diet). In contrast, *Lgals3*$^{-/-}$ CPZ mice exhibited remyelination only after CPZ removal (Fig. 1c). Similar results were obtained in the analysis of each CPZ-treated group relative to its own control, i.e., WT CPZ relative to WT C mice, and *Lgals3*$^{-/-}$ CPZ relative to *Lgals3*$^{-/-}$ C mice, which indicates that data are not altered by basal hypomyelination (Fig. 1e) and that both WT CPZ and *Lgals3*$^{-/-}$ CPZ mice reach the remyelination levels of their respective C groups at the end of the process (Fig. 1e). Western blot analyses of MBP expression provided support for immunohistochemical data and highlighted that not all MBP isoforms were equally altered, the 21.5 and 17.4 kDa isoforms being most affected (Fig. 1f).

For a deeper study of the remyelination process, changes in the numbers of CAII+ and CC1+ cells were analyzed as markers of different stages in oligodendroglial differentiation. In brain coronal slices from CC (Fig. 2a, b), the number of CAII+ cells decreased in both CPZ-treated groups during demyelination, with *Lgals3*$^{-/-}$ mice starting at a lower level than WT mice. During remyelination, the number of CAII+ cells recovered only by 50 % both in WT and *Lgals3*$^{-/-}$ mice (Fig. 2b). The same tendency was observed for CC1+ cells during demyelination, although recovery during remyelination appeared to be more efficient in *Lgals3*$^{-/-}$ mice (Fig. 2c, d), with the number of CC1+ cells reaching a higher WT CPZ/WT C ratio than did *Lgals3*$^{-/-}$ CPZ/*Lgals3*$^{-/-}$ C in week 8. It is worth pointing out that although there were no significant differences between WT CPZ and *Lgals3*$^{-/-}$ CPZ in the numbers of CAII+ and CC1+ cells at the peak of demyelination (week 5), these numbers were greater in WT CPZ than in *Lgals3*$^{-/-}$ CPZ mice 2 weeks after CPZ removal from the diet (week 8).

In turn, the number of OPCs labeled for PDGFRα was higher in CC in *Lgals3*$^{-/-}$ CPZ compared to WT CPZ during demyelination, as well as in *Lgals3*$^{-/-}$ C compared to WT C, which suggests a higher oligodendroglial proliferative response in *Lgals3*$^{-/-}$ mice, possibly due to their basal hypomyelination and their higher degree of demyelination. When both groups were allowed to remyelinate after CPZ removal, the number of PDGFRα+ cells decreased in both groups, but was more pronounced in WT mice, which reached levels nonsignificantly different from *Lgals3*$^{-/-}$ mice (Fig. 2e).

Interestingly, these cells were stellate, with a higher number of multipolar processes in the CC of WT mice both during demyelination and remyelination, which indicates a decreased ability of *Lgals3*$^{-/-}$ cells to differentiate. Quantitative support was obtained through the numbers and lengths of branches and terminal processes. OPCs from WT mice showed more branching, more ramification and, consequently, more ramification terminals than *Lgals3*$^{-/-}$ mice at weeks 5 and 8 (Fig. 2f).

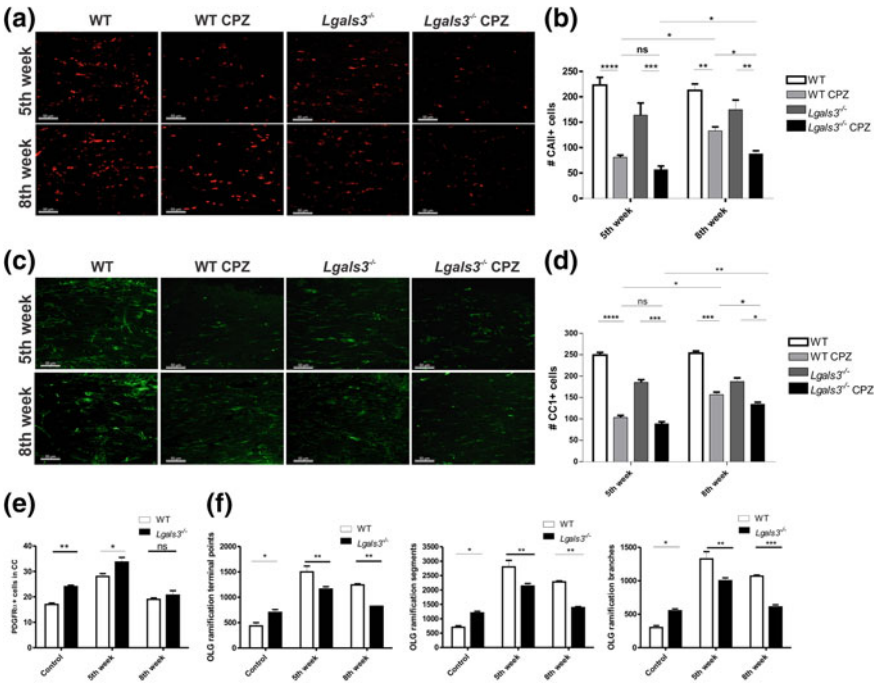

Fig. 2 **a** Identification of CAII+ cells in CC during demyelination and remyelination. **b** Quantification shows a decrease in the number of CAII+ cells during demyelination in both experimental groups, the decrease being greater in *Lgals3*$^{-/-}$ CPZ mice. Remyelination was not complete, as values were nonsignificantly corrected in comparison to demyelination. **c**, **d** Identification and quantification of CC1+ cells following the same procedures as in (**a**, **b**), respectively. Values represent the mean ± SEM of five independent experiments. *$p < 0.05$, **$p < 0.01$, ***$p < 0.001$ and ****$p < 0.0001$ using two-way ANOVA followed by Bonferroni post hoc tests. **e** OPCs identified as PDGFrα+ cells in the CC. Quantification revealed an increase in the number of PDGFrα+ cells in CC of *Lgals3*$^{-/-}$ CPZ mice versus WT CPZ during demyelination, with an important decrease in both conditions after remyelination. **f** Filament plot was performed for each image from CC sections, comparing PDGFrα+ cell arborization between demyelination and remyelination. Quantitative assessment of the filament plot exhibited greater arborization in WT CPZ than *Lgals3*$^{-/-}$ CPZ mice, both during demyelination and remyelination. Values represent the mean ± SEM of five independent experiments. *$p < 0.05$ and **$p < 0.01$ using two-way ANOVA followed by Bonferroni post hoc tests

Ultrastructural changes evaluated by EM in CC sections (Fig. 3a) showed that myelin was more loosely wrapped around axons in *Lgals3*$^{-/-}$ than in WT mice, and that this abnormal wrapping increased in both groups during CPZ-induced demyelination. Some of these abnormalities were solved during remyelination in WT CPZ but not in *Lgals3*$^{-/-}$ CPZ mice. Morphometric analyses showed that the number of myelinated axons per field increased in both groups from demyelination to remyelination, although more significantly in WT mice. Despite this increase, WT CPZ remyelination values nearly reached those of WT ($p = 0.3710$); this did

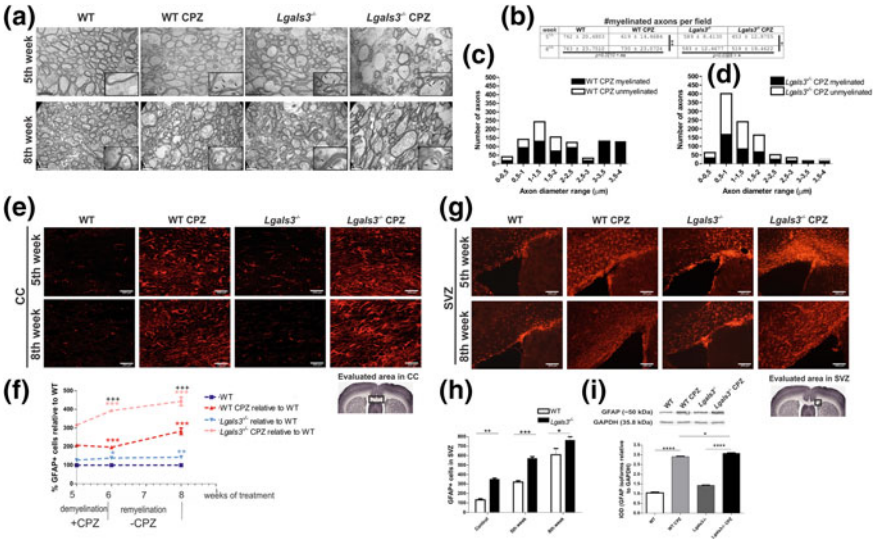

Fig. 3 **a** Representative electron micrographs at 6000× (scale bar equals 0.5 μm) from demyelinated and remyelinated axons. Each condition shows an *inset* with a highly magnified image (20000×) of a representative axon. Samples were taken in the zone highlighted in the *black box* in the scheme. As compared to that of WT mice, myelin observed in *Lgals3*$^{-/-}$ mice was loosely wrapped around the axons, an abnormality which was incremented during CPZ-induced demyelination and not solved during remyelination. *Black arrows* indicate loosely wrapped axon areas. **b** Table showing the percentage of correctly myelinated axons. Values represent the mean ± SEM *ns* non-significant, *$p < 0.05$ and **$p < 0.01$ using two-way ANOVA followed by Bonferroni post hoc tests. **c**, **d** Axon diameter frequency categorized by range (myelinated–demyelinated) comparing WT CPZ with WT, and *Lgals3*$^{-/-}$ CPZ with *Lgals3*$^{-/-}$ after remyelination. CPZ WT mice showed larger axons than WT, while *Lgals3*$^{-/-}$ mice exhibited similar axon size as *Lgals3*$^{-/-}$ CPZ. In both cases, there is evidence for similar patterns of axon size change between demyelination and remyelination. **e** Astrocytes immunolabeled with anti-GFAP antibody in the CC showed astrocytic activation in response to CPZ treatment in both types of animals during demyelination and its persistence in remyelination. *Bottom right* image indicates the area evaluated (*black box*, 40×). **f** Quantification of GFAP+ cells evaluated in relationship to the WT condition (set at 100 %). The increased astroglial response was particularly strong in *Lgals3*$^{-/-}$ mice in the last period of demyelination. During remyelination, the curve slopes were similar in the CPZ condition. Percentages of GFAP+ cells were relative to each WT. Both CPZ curves had a similar slope. **g** GFAP+ cells in the SVZ. Bottom right image indicates the area evaluated (*black box*, 40×). **h** Quantitative assessment of astrocytes in the SVZ. *Lgals3*$^{-/-}$ CPZ mice had more GFAP+ cells than CPZ WT mice in demyelination, but not during remyelination. **i** Western blot analysis of GFAP expression in the CC at the 8th week. The graph shows GFAP levels relative to GAPDH. Values represent the mean ± SEM of five independent experiments. *ns* non-significant, *$p < 0.05$, **$p < 0.01$ and ***$p < 0.001$ using two-way ANOVA followed by Bonferroni post hoc tests

not occur for *Lgals3*$^{-/-}$ CPZ mice ($p = 0.0328$) (Fig. 3b). When data were analyzed discriminating for axon diameter and myelination status, results in *Lgals3*$^{-/-}$ mice showed an increase in the number of small axons at the expense of a decrease in the number of large ones, both among myelinated and unmyelinated axons (Fig. 3d).

Astrocytic Activation Persists in Remyelinated Mice Despite CPZ Removal and Was More Pronounced in Lgals3$^{-/-}$ Mice

Astrocytes immunelabeled with anti-GFAP antibody in the CC showed there was reactive astrogliosis in response to CPZ treatment in both groups during demyelination, with more pronounced levels in *Lgals3*$^{-/-}$ mice, in agreement with previous results (Hoyos et al. 2014). This effect persisted during remyelination, and the differences between animal types became more noticeable (Fig. 3e). The quantification of GFAP+ cells, setting the WT condition at 100 %, showed an increase in astroglial response, especially in *Lgals3*$^{-/-}$ and particularly at the critical point (5 weeks) of demyelination (Fig. 3f). The analysis of GFAP+ cells in the SVZ (Fig. 3g) revealed a larger amount in *Lgals3*$^{-/-}$ CPZ than in WT CPZ mice during demyelination, a difference that remained statistically significant during remyelination (Fig. 3h). Support for these results was obtained from Western blot analyses of GFAP expression at week 8 (Fig. 3i).

Gal-3 Could Be Critical for MMP-3 Expression

Immunohistochemical studies revealed a pronounced increase in the expression levels of MMP-3 in WT CPZ at 5 weeks, the critical point of demyelination, and after 2 weeks of remyelination. This increase was almost absent in *Lgals3*$^{-/-}$ mice, which indicates that Gal-3 could be critical for MMP-3 expression. MMP-3 was mainly detected in microglia, identified as Iba+ cells (Fig. 4a), and quantitative support was obtained through the determination of MMP-3 IOD in the CC in the different experimental situations (Fig. 4b).

Only WT Mice Exhibit Changes in the Microglial Phagocytic Phenotype During Remyelination

The total number of microglia evaluated through Iba-1 immunelabeling decreased during remyelination in both WT and *Lgals3*$^{-/-}$ mice (Fig. 5a and b). Ramification values also decreased in both WT and *Lgals3*$^{-/-}$ mice (Fig. 5c).

However, the number of CD45+ cells during remyelination showed a significant decrease only in WT mice. Similar results were obtained for TNF and TREM-2 expression, which displayed a significant decrease after remyelination only in WT mice. In contrast, the number of CD11b^{+} cells decreased during remyelination in both mouse types (Fig. 6a), in agreement with the results obtained for Iba+ cells. There were no differences across experimental groups or conditions in neutrophil migration in response to CPZ intoxication or Gal-3 depletion (Fig. 6b).

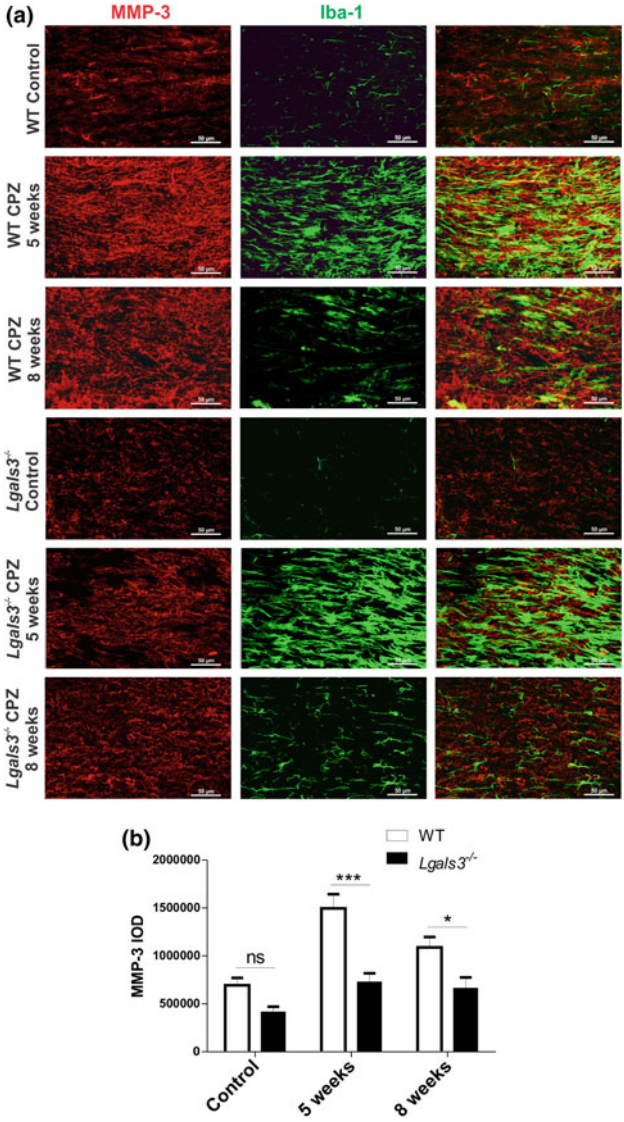

Fig. 4 **a** Representative sections showing MMP-3 and Iba-1 in CC (40×). During demyelination, there was an increase in MMP-3 protein (*red*) in the CC of WT mice, which was even greater during remyelination. The increase in MMP-3 in *Lgals3*$^{-/-}$ mice represented 50 % of that found in WT mice. During remyelination in WT mice and demyelination in *Lgals3*$^{-/-}$ mice, MMP-3 co-localized with microglia (Iba-1+ cells in *green*). **b** MMP-3 in WT and *Lgals3*$^{-/-}$ mice during demyelination–remyelination

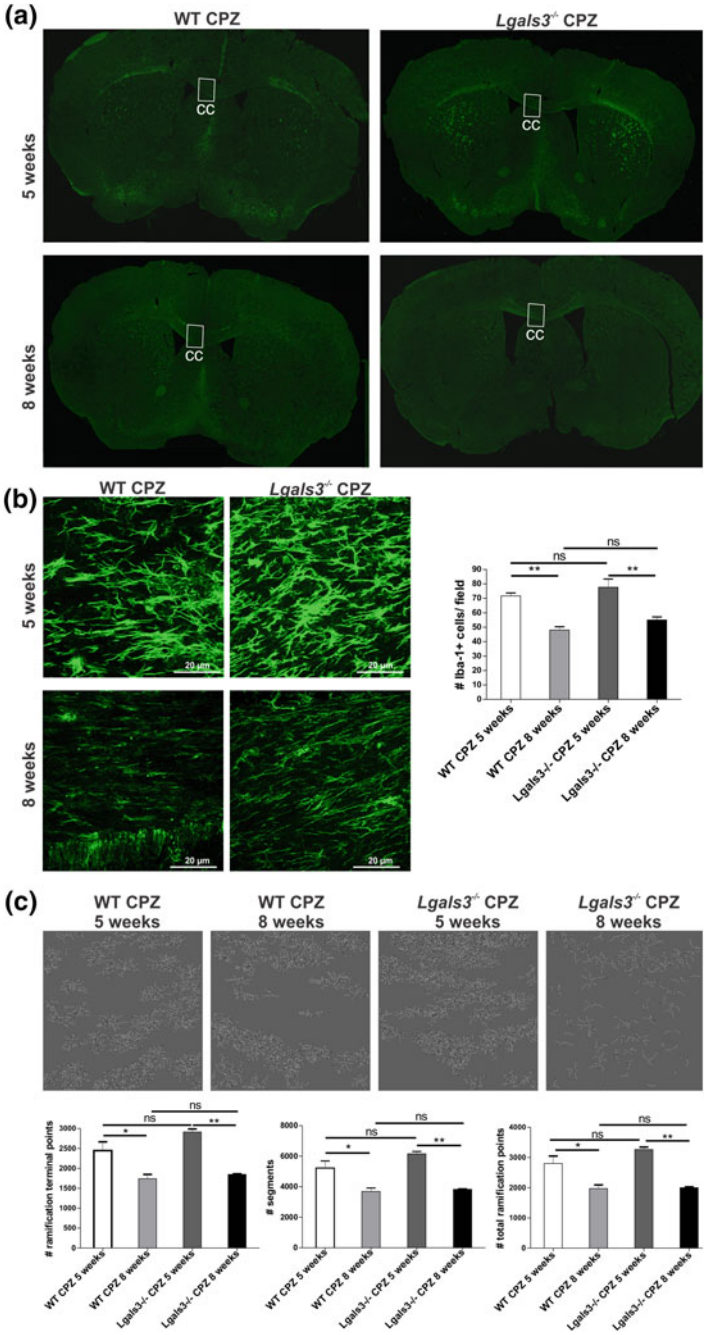
(a)
WT CPZ
Lgals3-/- CPZ
5 weeks
8 weeks
CC
(b)
WT CPZ
Lgals3-/- CPZ
5 weeks
8 weeks
20 µm
Iba-1+ cells/ field
ns
**
WT CPZ 5 weeks
WT CPZ 8 weeks
Lgals3-/- CPZ 5 weeks
Lgals3-/- CPZ 8 weeks
(c)
WT CPZ 5 weeks
WT CPZ 8 weeks
Lgals3-/- CPZ 5 weeks
Lgals3-/- CPZ 8 weeks
ramification terminal points
segments
total ramification points
ns
*
**

◀ **Fig. 5** **a** Immunolabeled for Iba-1 in coronal brain slices during demyelination–remyelination in WT and *Lgals3*$^{-/-}$ mice. **b** Iba-1 immunohistochemistry in the CC of WT and *Lgals3*$^{-/-}$ mice during demyelination–remyelination. Quantification of Iba+ cells. **c** Filament plot for all experimental conditions. Quantification of total ramification, ramification segments and terminal points under the same conditions as mentioned above. Values represent the mean ± SEM of five independent experiments. *ns* non-significant, *$p < 0.05$, **$p < 0.01$ and ***$p < 0.001$ using two-way ANOVA followed by Bonferroni post hoc tests

Behavioral Performance After Remyelination Reached Pre-CPZ-Intoxication Levels in Both Mouse Strains

After 2 weeks of recovery, both WT and *Lgals3*$^{-/-}$ mice significantly increased the number of total arm entries ($p < 0.05$), the percentage of open arm entries ($p < 0.001$) and the percentage of time spent in open arms ($p < 0.001$) (Fig. 6c). These data suggest that, at this point in treatment, WT and *Lgals3*$^{-/-}$ mice present lower levels of innate anxiety than their naïve counterparts. The WT recovery group also showed an augmented number of counts in the locomotor activity test ($p < 0.001$) (Fig. 6d), which reflects increased locomotion. On the other hand, WT and *Lgals3*$^{-/-}$ recovering mice showed no significant changes in the number of total arm entries or in the percentage of spontaneous alternations in the Y-maze test ($p < 0.05$) (Fig. 6e).

Discussion

Following the description of Gal-3 participation in the demyelination process (Hoyos et al. 2014), the present work was undertaken to gain insight into the role of Gal-3 in the remyelination process using a CPZ-induced demyelination model in C57BL/6 control and *Lgals3*$^{-/-}$ mice. CPZ emerges as one of the most suitable models available to investigate remyelination for several reasons: first, it is simple and easy to reproduce and entails low mortality (Kipp et al. 2009); second, the absence of peripheral inflammatory cells within the demyelinated lesion, such as lymphocytes or monocytes, leads to immune-independent demyelination/remyelination (McMahon et al. 2002; Remington et al. 2007; Ransohoff and Brown 2012); third and last, nearly complete remyelination allows for the study of the mechanisms underlying successful regeneration.

When demyelination is detected in this model, increased number of microglia and astrocytes are observed within the lesion (Matsushima and Morell 2001), which indicates that glial cells play a role both in demyelination and in remyelination. Reactive glia are now recognized to mediate complex processes, including

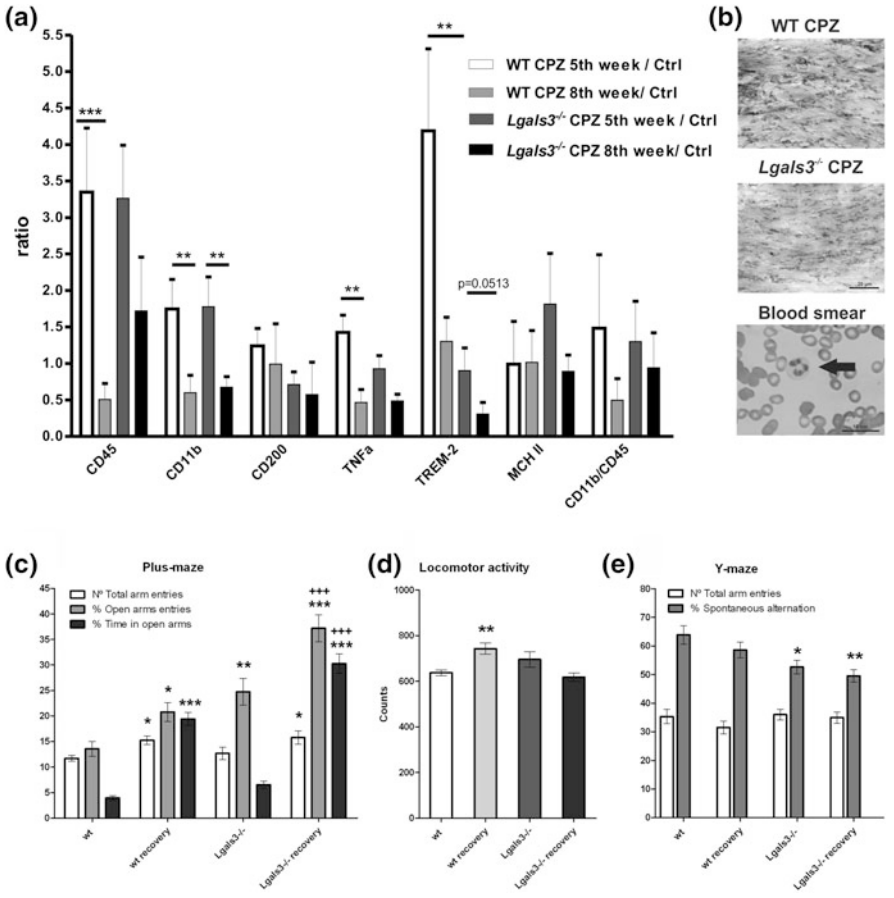

Fig. 6 **a** Flow cytometry analysis of cell surface receptors and cytokine production by pre-sorted microglial cells (CD11b+) from CC after remyelination. CD11b+ cells were purified by magnetic micro beads conjugated to an antibody against CD11b, followed by immunolabeling with a specific antibody against cell surface receptors and cytokines, and evaluated by flow cytometry. Data were processed with Winmdi 2.8 software. Pre-immune sera were used as negative controls for polyclonal antibodies. Isotype controls were used for specific monoclonal antibodies. At least 6 mice were analyzed per experimental condition at each time point. Values represent the mean ± SEM. ns: non-significant, $*p < 0.05$, $**p < 0.01$ and $***p < 0.001$ using two-way ANOVA followed by Bonferroni post hoc tests. **b** Neutrophil evaluation was done using May Grünwald Giemsa staining in samples of CC from WT and *Lgals3*$^{-/-}$ mice treated with CPZ. Magnification 60×. **c**–**e** Performance of WT and *Lgals3*$^{-/-}$ mice after 2-week remyelination in the plus maze, locomotor activity and Y-maze tests. Results are expressed as the mean ± SEM of (**c**) total arm entries, percentage of open arm entries and percentage of time spent in open arms measured in the plus maze test; **d** locomotor activity counts; and **e** total arm entries and percentage of spontaneous alternation measured in the Y-maze assay. Eight to fifteen animals were analyzed per group. $*p < 0.05$, $**p < 0.01$ and $***p < 0.001$ significantly different from WT mice and $^{+++}p < 0.001$ significantly different from *Lgals3*$^{-/-}$ mice, using Newman-Keuls Multiple Comparison Test after one-way ANOVA

beneficial and deleterious effects of brain injury and in neurodegeneration. Previous studies have investigated the microglial phenotype during remyelination by performing genome-wide gene expression analyses of microglia from the CC during demyelination and remyelination in the CPZ mouse model (Olah et al. 2012; Voss et al. 2012). They provide evidence for the existence of a microglial phenotype that supports remyelination as early as the onset of demyelination and continuing throughout remyelination. Transcriptomic analyses of the remyelination-supportive microglial phenotype indicate that microglia maintain tissue homeostasis and promote regeneration.

As previously discussed in Chapters "Glial cells and Integrity of the Nervous System", "Microglia Function in the Normal Brain", and "Purine Signaling and Microglial Wrapping", microglia release either neurotoxic or pro-recovery factors, depending on whether they are differentiated toward an M1 or M2 phenotype. They are involved in many types of inflammatory processes in the brain (Hanisch and Kettenmann 2007; David and Kroner 2011) and have also been proposed to participate in the initial stages of MS. Microglia also support cell survival during tissue repair after injury to the CNS (David and Kroner 2011). Moreover, Gal-3 is required for resident microglia activation and proliferation in response to ischemic injury (Lalancette-Hébert et al. 2012). A pronounced increase in the phagocytic capacity of microglial cells during CPZ-induced demyelination is associated mainly with an upregulation of the phagocytic receptor TREM-2b in WT but not in *Lgals3*$^{-/-}$ mice (Hoyos et al. 2014). These experiments have been now replicated during remyelination, showing a significant decrease in the number of CD45+, TNFα+ and TREM-2b+ cells in WT mice but no change in *Lgals3*$^{-/-}$ mice from demyelination (5 weeks) to remyelination (7 weeks) points.

Our recently published results on demyelination (Hoyos et al. 2014) show that OPCs generated in response to CPZ-induced demyelination in *Lgals3*$^{-/-}$ mice have a decreased ability to differentiate, which could be due to the inhibitory effects of impaired phagocytosis of myelin debris in *Lgals3*$^{-/-}$ microglia (Hoyos et al. 2014). Moreover, this could also be explained by our previous findings that conditioned media from Gal-3-expressing (but not *Lgals3*$^{-/-}$) microglia promote OLG differentiation (Pasquini et al. 2011). Previous papers have demonstrated that an interruption in OPC differentiation might be the reason for remyelination failure (Franklin et al. 2008; Ulrich et al. 2008). Therefore, *Lgals3*$^{-/-}$ mice could show a delay in remyelination due to a failure in Gal-3-induced OPC differentiation. Moreover, as *Lgals3*$^{-/-}$ mouse remyelination occurs in an environment poorly conditioned by microglia, myelin generated de novo is aberrant and appears loosely wrapped around axons. This could explain the behavioral deficit observed in these animals after remyelination, which will be discussed below.

Depending on various scenarios, astrocytes can either promote neuroplasticity or secrete inhibitory matrix molecules that suppress axonal growth. Some authors have postulated that astrocytes produce chemoattractants for OPCs, allowing them to

migrate from their resting positions toward the demyelination zone (Williams et al. 2007). This is probably the best explanation for the larger number of astrocytes in remyelination than in demyelination in both animal strains. However, *Lgals3*$^{-/-}$ mice reach higher levels of GFAP+ cells than WT littermates, which could reflect more severe demyelination.

While demyelination renders a significant reduction in axon caliber and a loss of small axons in *Lgals3*$^{-/-}$ mice after CPZ administration (Hoyos et al. 2014), remyelination generates a greater recovery in WT mice than in *Lgals3*$^{-/-}$ mice in small axons, which again indicates a failure in the remyelination process in the absence of Gal-3. It is presumably the more abundant presence of small-caliber axons that accounts for the incomplete remyelination observed in *Lgals-3*$^{-/-}$ mice. It has been suggested that the reduction in axon caliber after initial demyelination is largely reversible upon remyelination (Mason et al. 2001), but those axons that do not remyelinate remain small in caliber. Small-caliber axons are probably initially abundant in *Lgals-3*$^{-/-}$ mice and never become myelinated.

As already discussed in this chapter, the 21.5 kDa MBP isoform is the first to be synthesized; it promotes not only proliferation but also branching of OPCs (Smith et al. 2013). MBP isoforms including 18.2 and 14.0 kDa are involved in myelin compaction and stabilization (Chernoff 1981). During demyelination, a dramatic decrease in the 21.5 kDa MBP isoform is observed in the absence of Gal-3, which explains the deficit in normal myelin formation (Pasquini et al. 2011). During remyelination, *Lgals3*$^{-/-}$ mice do not seem to recover expression of the 21.5 and 18.2 kDa isoforms, which might explain abnormal remyelination.

In a variety of demyelinating diseases, there is a well-established role for MMPs, a family of extracellular endopeptidases for tissue remodeling and regeneration (Yong et al. 2001). MMPs cleave all components of the extracellular matrix and thereby serve important homeostatic functions. During oligodendrogenesis and remyelination, OPC can also release multiple factors to modulate neighboring cells and their environment. Gal-3 is readily cleaved by MMPs, thus altering its own carbohydrate-binding activity (Ochieng et al. 1994). We have demonstrated that Gal-3 is cleaved by MMP-2 in OPC but not in differentiated OLG (Pasquini et al. 2011). In this situation, and as described in our previous work, MMP-3 is upregulated during CPZ treatment, while Gal-3 seems to be necessary to upregulate the expression of MMP-3 and to promote microglial activation. As previously demonstrated, MMP-3 could mediate mature OLG apoptosis and microglial activation (Kim and Joh 2006). These authors have also proved that the catalytically active form of MMP-3 (actMMP-3) is released from apoptotic PC12 cells grown in serum-deprived medium. ActMMP-3 leads to the production of microglial inflammatory cytokines such as TNF through the ERK-NFκB signal transduction pathway, which in turn exacerbates neural cell degeneration.

Behavioral observations from three different approaches (plus maze, locomotor activity, and Y-maze tests) evidence changes in anxiety responses to the challenge of novelty and height, motor performance, and spatial working memory activity. We have previously demonstrated that Lgals3$^{-/-}$ mice exhibit decreased anxiety

consistent with abnormalities in their myelin structure (Pasquini et al. 2011) and that CPZ treatment induces more pronounced demyelination in Lgals3-/- relative to WT mice (Hoyos et al. 2014). In the current study, after the recovery period of 2 weeks, a decrease in anxiety persisted both for WT and Lgals3$^{-/-}$ mice, as evidenced by augmented percentages of entries and time spent in open arms in the plus maze test. Locomotor activity showed an increase in the locomotor activity counts as well as in the number of total arm entries in the plus maze test. Meanwhile, spatial working memory was reestablished, as compared to their untreated counterparts. Similar behavioral performance was expected of recovering mice and their naïve counterparts. However, the recovery group showed higher open arms activity in the plus maze and augmented locomotion than untreated animals. These data suggest that some capabilities are altered even when histological analyses evidence fiber remyelination. Previous studies have already found that CPZ-fed mice display abnormal behavior during the demyelination process with partial recovery of functions during the remyelination period, with enhanced locomotor activity, improved spatial working memory, and decreased anxiety levels (Stancic et al. 2012; Franco-Pons et al. 2007; Xu et al. 2009). Our results indicate that behavioral deficits follow the course of demyelination–remyelination-induced by CPZ administration, and that some of the changes persist and seem to be irreversible even 2 weeks after CPZ withdrawal.

Remyelination is a key mechanism which restores myelin to normal conditions after demyelination and which seems to be importantly regulated by Gal-3, a molecule participating in OPC differentiation. Since Gal-3 is expressed in microglia, myelin restoration could be mediated by the Gal-3-induced M2 cell polarization, or by Gal-3 acting directly on OPC differentiation. In conclusion, our findings demonstrate that Gal-3 hierarchically governs the myelination process, at least in the CPZ model, through the modulation of microglial cells, MMP activity, and myelin architecture.

References

Chandler S, Coates R, Gearing A, Lury J, Wells G, Bone E (1995) Matrix metalloproteinases degrade myelin basic protein. Neurosci Lett 201:223–226

Chandler S, Cossins J, Lury J, Wells G (1996) Macrophage metalloelastase degrades matrix and myelin proteins and processes a tumour necrosis factor-alpha fusion protein. Biochem Biophys Res Commun 228:421–429

Chernoff GF (1981) Shiverer: an autosomal recessive mutant mouse with myelin deficiency. J Hered 72:128

David S, Kroner A (2011) Repertoire of microglial and macrophage responses after spinal cord injury. Nat Rev Neurosci 12:388–399

Franco-Pons N, Torrente M, Colomina MT, Vilella E (2007) Behavioral deficits in the cuprizone-induced murine model of demyelination/remyelination. Toxicol Lett 169:205–213

Franklin RJ, Ffrench-Constant C (2008) Remyelination in the CNS: from biology to therapy. Nat Rev Neurosci 11:839–855

Franklin RJ, Kotter MR (2008) The biology of CNS remyelination: the key to therapeutic advances. J Neurol 255:19–25

Hanisch UK, Kettenmann H (2007) Microglia: active sensor and versatile effector cells in the normal and pathologic brain. Nat Neurosci 10:1387–1394

Hansmann F, Herder V, Kalkuhl A, Haist V, Zhang N, Schaudien D, Deschl U, Baumgärtner W, Ulrich R (2012) Matrix metalloproteinase-12 deficiency ameliorates clinical course and demyelination in Theiler's murine encephalomyelitis. Acta Neuropathol 124:127–142

Hoyos HC, Rinaldi M, Mendez-Huergo SP, Marder M, Rabinovich GA, Pasquini JM, Pasquini LA (2014) Galectin-3 controls the response of microglial cells to limit cuprizone-induced demyelination. Neurobiol Dis 62:441–455

Hsu DK, Yang RY, Pan Z, Yu L, Salomon DR, Fung-Leung WP, Liu FT (2000) Targeted disruption of the galectin-3 gene results in attenuated peritoneal inflammatory responses. Am J Pathol 156:1073–1083

Jiang HR, Al Rasebi Z, Mensah-Brown E, Shahin A, Xu D, Goodyear CS, Fukada SY, Liu FT, Liew FY, Lukic ML (2009) Galectin-3 deficiency reduces the severity of experimental autoimmune encephalomyelitis. J. Immunol 182:1167–1173

Kim YS, Joh TH (2006) Microglia, major player in the brain inflammation: their roles in the pathogenesis of Parkinson's disease. Exp Mol Med 38:333–347

Kipp M, Clarner T, Dang J, Copray S, Beyer C (2009) The cuprizone animal model: new insights into an old story. Acta Neuropathol 118:723–736

Kotter MR, Li WW, Zhao C, Franklin RJ (2006) Myelin impairs CNS remyelination by inhibiting oligodendrocyte precursor cell differentiation. J Neurosci 26:328–332

Lalancette-Hébert M, Swarup V, Beaulieu JM, Bohacek I, Abdelhamid E, Weng YC, Sato S, Kriz J (2012) Galectin-3 is required for resident microglia activation and proliferation in response to ischemic injury. J Neurosci 32:10383–10395

Li Y, Komai-Koma M, Gilchrist DS, Hsu DK, Liu FT, Springall T, Xu D (2008) Galectin-3 is a negative regulator of lipopolysaccharide-mediated inflammation. J Immunol 181:2781–2789

Mason JL, Langaman C, Morell P, Suzuki K, Matsushima GK (2001) Episodic demyelination and subsequent remyelination within the murine central nervous system: changes in axonal calibre. Neuropathol Appl Neurobiol 27:50–58

Masuda-Nakagawa LM, Muller KJ, Nicholls JG (1993) Axonal sprouting and laminin appearance after destruction of glial sheaths. Proc Natl Acad Sci USA 90(11):4966–4970

Matsushima GK, Morell P (2001) The neurotoxicant cuprizone as a model to study demyelination and remyelination in the central nervous system. Brain Pathol 11:107–116

McMahon EJ, Suzuki K, Matsushima GK (2002) Peripheral macrophage recruitment in cuprizone-induced CNS demyelination despite an intact blood–brain barrier. J Neuroimmunol 130:32–45

Mok SW, Thelen KM, Riemer C, Bamme T, Gültner S, Lütjohann D, Baier M (2006) Simvastatin prolongs survival times in prion infections of the central nervous system. Biochem Biophys Res Commun 348:697–702

Mok SW, Riemer C, Madela K, Hsu DK, Liu FT, Gültner S, Heise I, Baier M (2007) Role of galectin-3 in prion infections of the CNS. Biochem Biophys Res Commun 359:672–678

Ochieng J, Fridman R, Nangia-Makker P, Kleiner DE, Liotta LA, Stetler-Stevenson WG, Raz A (1994) Galectin-3 is a novel substrate for human matrix metalloproteinases-2 and -9. Biochemistry 33:14109–14114

Olah M, Amor S, Brouwer N, Vinet J, Eggen B, Biber K, Boddeke HW (2012) Identification of a microglia phenotype supportive of remyelination. Glia 60:306–321

Pasquini LA, Millet V, Hoyos HC, Giannoni JP, Croci DO, Marder M, Liu FT, Rabinovich GA, Pasquini JM (2011) Galectin-3 drives oligodendrocyte differentiation to control myelin integrity and function. Cell Death Differ 18:1746–1756

Rabinovich GA, Croci DO (2012) Regulatory circuits mediated by lectin–glycan interactions in autoimmunity and cancer. Immunity 36:322–335

Rabinovich GA, Toscano MA (2009) Turning 'sweet' on immunity: galectin-glycan interactions in immune tolerance and inflammation. Nat Rev Immunol 9:338–352

Rabinovich GA, Toscano MA, Jackson SS, Vasta GR (2007) Functions of cell surface galectin glycoprotein lattices. Curr Opin Struct Biol 17:513–520

Ransohoff RM, Brown MA (2012) Innate immunity in the Central Nervous System. J Clin Invest 122:1164–1171

Remington LT, Babcock AA, Zehntner SP, Owens T (2007) Microglial recruitment, activation, and proliferation in response to primary demyelination. Am J Pathol 170:1713–1724

Riemer C, Neidhold S, Burwinkel M, Schwarz A, Schultz J, Krätzschmar J, Mönning U, Baier M (2004) Gene expression profiling of scrapie-infected brain tissue. Biochem Biophys Res Commun 323:556–564

Shiryaev SA, Savinov AY, Cieplak P, Ratnikov BI, Motamedchaboki K, Smith JW, Strongin AY (2009) Matrix metalloproteinase proteolysis of the myelin basic protein isoforms is a source of immunogenic peptides in autoimmune multiple sclerosis. PLoS One 4(3):e4952

Skuljec J, Gudi V, Ulrich R, Frichert K, Yildiz O, Pul R, Voss EV, Wissel K, Baumgärtner W, Stangel M (2011) Matrix metalloproteinases and their tissue inhibitors in cuprizone-induced demyelination and remyelination of brain white and gray matter. J Neuropathol Exp Neurol 70:758–769

Smith GS, Sambroska B, Hawley SP, Klaiman JM, Gillis TE, Jones N, Boggs JM, Harauz G (2013) Nucleus-localized 21.5-kDa myelin basic protein promotes oligodendrocyte proliferation and enhances neurite outgrowth in coculture, unlike the plasma membrane-associated 18.5-kDa isoform. J Neurosci Res 91:349–362

Stadelmann C (2011) Multiple sclerosis as a neurodegenerative disease: pathology, mechanisms and therapeutic implications. Curr Opin Neurol 24:224–229

Stancic M, Slijepcevic D, Nomden A, Vos MJ, de Jonge JC, Sikkema AH, Gabius HJ, Hoekstra D, Baron W (2012) Galectin-4, a novel neuronal regulator of myelination. Glia 60:919–935

Ulrich R, Gerhauser I, Seeliger F, Baumgärtner W, Alldinger S (2005) Matrix metalloproteinases and their inhibitors in the developing mouse brain and spinal cord: A reverse transcription quantitative polymerase chain reaction study. Dev Neurosci 27:408–418

Ulrich R, Baumgärtner W, Gerhauser I, Seeliger F, Haist V, Deschl U, Alldinger S (2006) MMP-12, MMP-3, and TIMP-1 are markedly upregulated in chronic demyelinating Theiler murine encephalomyelitis. J Neuropathol Exp Neurol 65:783–793

Ulrich R, Seeliger F, Kreutzer M, Germann PG, Baumgärtner W (2008) Limited remyelination in Theiler's murine encephalomyelitis due to insufficient oligodendroglial differentiation of nerve/glial antigen 2 (NG2)-positive putative oligodendroglial progenitor cells. Neuropathol Appl Neurobiol 34:603–620

von Bernhardi R, Muller KJ (1995) Repair of the central nervous system: lessons from lesions in leeches. J Neurobiol 27(3):353–366

Voss EV, Škuljec J, Gudi V, Skripuletz T, Pul R, Trebst C, Stangel M (2012) Characterisation of microglia during de- and remyelination: can they create a repair promoting environment? Neurobiol Dis 45:519–528

Williams A, Piaton G, Lubetzki C (2007) Astrocytes-friends or foes in multiple sclerosis? Glia 55:1300–1312

Xu H, Yang HJ, Zhang Y, Clough R, Browning R, Li XM (2009) Behavioral and neurobiological changes in C57BL/6 mice exposed to cuprizone. Behav Neurosci 123:418–429

Yang RY, Rabinovich GA, Liu FT (2008) Galectins: structure, function and therapeutic potential. Expert Rev Mol Med 10:e17

Yong VW, Power C, Forsyth P, Edwards DR (2001) Metalloproteinases in biology and pathology of the nervous system. Nat Rev Neurosci 7:502–511